

# Galaxy And Mass Assembly (GAMA) Blended Spectra Catalog: Strong Galaxy-Galaxy Lens and Occulting Galaxy Pair Candidates.

B.W. Holwerda<sup>1\*</sup>, I. K. Baldry<sup>2</sup>, M. Alpaslan<sup>3</sup>, A. Bauer<sup>4</sup>, J. Bland-Hawthorn<sup>5</sup>,  
S. Brough<sup>4</sup>, M. J. I. Brown<sup>6</sup>, M. E. Cluver<sup>7</sup>, C. Conselice<sup>8</sup>, S.P. Driver<sup>9,10</sup>,  
A.M. Hopkins<sup>4</sup>, D. H. Jones<sup>11</sup>, Á.R. López-Sánchez<sup>4,11</sup>, J. Loveday<sup>12</sup>, M.J. Meyer<sup>9</sup>,  
and A. Moffett<sup>9</sup>

<sup>1</sup> *University of Leiden, Sterrenwacht Leiden, Niels Bohrweg 2, NL-2333 CA Leiden, The Netherlands*

<sup>2</sup> *Astrophysics Research Institute, Liverpool John Moores University, IC2, Liverpool Science Park, 146 Brownlow Hill, Liverpool, L3 5RF, UK*

<sup>3</sup> *NASA Ames Research Centre, N232, Moffett Field, Mountain View, CA 94034, USA*

<sup>4</sup> *Australian Astronomical Observatory, 105 Delhi Rd. North Ryde NSW 2113*

<sup>5</sup> *Sydney Institute for Astronomy, School of Physics A28, University of Sydney, NSW 2006, Australia*

<sup>6</sup> *School of Physics, Monash University, Clayton, Vic 3800, Australia*

<sup>7</sup> *Department of Physics, University of the Western Cape, Robert Sobukwe Road, Bellville, 7530, South Africa*

<sup>8</sup> *University of Nottingham, School of Physics & Astronomy, Nottingham, NG7 2RD UK*

<sup>9</sup> *ICRAR M468, University of Western Australia, 35 Stirling Hwy, Crawley WA 6009 Australia*

<sup>10</sup> *School of Physics & Astronomy, University of St Andrews, North Haugh, St Andrews, KY16 9SS, Scotland*

<sup>11</sup> *Department of Physics and Astronomy, Macquarie University, NSW 2109, Australia*

<sup>12</sup> *Astronomy Centre, University of Sussex, Falmer, Brighton BN1 9QH*

submitted to MNRAS, February 2015

## ABSTRACT

We present the catalogue of blended galaxy spectra from the Galaxy And Mass Assembly (GAMA) survey. These are cases where light from two galaxies are significantly detected in a single GAMA fibre. Galaxy pairs identified from their blended spectrum fall into two principal classes: they are either strong lenses, a passive galaxy lensing an emission-line galaxy; or occulting galaxies, serendipitous overlaps of two galaxies, of any type. Blended spectra can thus be used to reliably identify strong lenses for follow-up observations (high resolution imaging) and occulting pairs, especially those that are a late-type partly obscuring an early-type galaxy which are of interest for the study of dust content of spiral and irregular galaxies. The GAMA survey setup and its AUTOZ automated redshift determination were used to identify candidate blended galaxy spectra from the cross-correlation peaks. We identify 280 blended spectra with a minimum velocity separation of 600 km/s, of which 104 are lens pair candidates, 71 emission-line-passive pairs, 78 are pairs of emission-line galaxies and and 27 are pairs of galaxies with passive spectra. We have visually inspected the candidates in the Sloan Digital Sky Survey (SDSS) and Kilo Degree Survey (KiDS) images. Many blended objects are ellipticals with blue fuzz (*Ef* in our classification). These latter “Ef” classifications are candidates for possible strong lenses, massive ellipticals with an emission-line galaxy in one or more lensed images. The GAMA lens and occulting galaxy candidate samples are similar in size to those identified in the entire SDSS. This blended spectrum sample stands as a testament of the power of this highly complete, second-largest spectroscopic survey in existence and offers the possibility to expand e.g., strong gravitational lens surveys.

**Key words:** catalogues galaxies: statistics galaxies: distances and redshifts (ISM:) dust, extinction gravitational lensing: strong

\* E-mail: holwerda@strw.leidenuniv.nl, Twitter: @benneholw-

## 1 INTRODUCTION

Interstellar dust is still a dominant astrophysical unknown in cosmological distance estimates (Albrecht et al. 2006; Holwerda 2008; Holwerda et al. 2014) and models of how starlight is re-processed within a galaxy (e.g., Baes et al. 2010; Bianchi & Xilouris 2011; Popescu et al. 2011; de Looze et al. 2012; Holwerda et al. 2012b) because some 10-30% of all the starlight is re-emitted by the dust in the far-infrared (Popescu et al. 2000). Interstellar dust can be found in two ways; by its emission or through the extinction of stellar light.

Characterization of emission has made great strides with the *Spitzer* and *Herschel Space Observatories* (e.g., Hinz et al. 2009, 2012; Bendo et al. 2012, 2014; Smith et al. 2010; Baes et al. 2010; Xilouris et al. 2012; Galametz et al. 2012; Draine et al. 2014; Verstappen et al. 2013; Hughes et al. 2014a,b). A library of far-infrared and sub-mm images of nearby galaxies is currently being collated and more insight into the physics and distribution of interstellar dust in nearby galaxies can be expected with the great improvements in spectral coverage, sensitivity and spatial resolution.

Extinction measures of dust have some specific advantages over emission: they do not depend on the dust temperature, allowing for the detection of much colder dusty structures, and typically have the high resolution of the optical imaging observations. The single drawback is that one needs a known background light source. In the case of the transparency of spiral galaxies, two techniques have just such a proven background source: background galaxies counts and occulting galaxy pairs. The technique that uses the number of background galaxies (Cuillandre et al. 2001; González et al. 1998, 2003; Holwerda 2005; Holwerda et al. 2005a,b,c,d,e, 2007a,c, 2012a) is nearing obsolescence as its inherent resolution and accuracy, limited by the intrinsic cosmic variance of background sources, are now surpassed by the accuracy and sensitivity of *Herschel Space Observatory* observations of dust surface density in nearby galaxies.

The occulting galaxies technique, however, has increased steadily in accuracy and usefulness, owing in a large part to the increasing sample sizes. Estimating dust extinction and mass from differential photometry in occulting pairs of galaxies was first proposed by White & Keel (1992). Their technique was then applied to all known pairs using ground-based optical images (Andredakis & van der Kruit 1992; Berlind et al. 1997; Domingue et al. 1999; White et al. 2000) and spectroscopy (Domingue et al. 2000). Subsequently, some pairs were imaged with the *Hubble Space Telescope* (HST Keel & White 2001a,b; Elmegreen et al. 2001; Holwerda et al. 2009; Holwerda & Keel 2013). These initial results, however, were limited by sample sizes ( $\sim 15$  pairs). More recently, new pairs were found in the SDSS spectroscopic catalogue (86 pairs in Holwerda et al. 2007b) and through the GalaxyZOO project (Lintott et al. 2008): 1993 pairs reported in Keel et al. (2013). This wealth of new pairs provided opportunities for follow-up with IFU observations (Holwerda et al. 2013; Holwerda & Keel 2013) and GALEX (Keel et al. 2014). A greatly expanded occulting galaxy catalog improves accuracy as “ideal pairs” – an elliptical partially occulted by a late-type galaxy – can be selected

for follow-up. Ellipticals are the optimal background source as their light profile is smooth and very symmetric<sup>1</sup>.

Results from the occulting galaxy pairs include: (1) a mean extinction profile (White et al. 2000; Domingue et al. 2000; Holwerda et al. 2007b), (2) an indication that the dust may be fractal (Keel & White 2001a) and (3) the observation that the colour-extinction relation is grey, i.e. there is little or no relation between the reddening of the stellar populations and total extinction. The latter is due to the coarse physical sampling of ground-based observations. The Galactic Extinction Law returns as soon as the physical sampling of the overlap region resolves the molecular clouds in the foreground disk ( $< 100$  pc Keel & White 2001a,b; Elmegreen et al. 2001; Holwerda et al. 2009).

A very reliable way to identify occulting galaxy pairs, i.e., purely serendipitous overlaps of galaxies is through blended spectra. In Holwerda et al. (2007b), we used the rejects from the Strong Lenses with ACS Survey (SLACS Bolton et al. 2004, 2006), a highly successful search for strong lenses, confirmed with HST (Treu et al. 2006; Koopmans et al. 2006; Gavazzi et al. 2007; Bolton et al. 2008a; Gavazzi et al. 2008; Bolton et al. 2008b; Treu et al. 2009), with spectroscopic selection extended now to the BOSS survey (Brownstein et al. 2012; Bolton et al. 2012). Both types of blended spectral sources have two things in common: very close association on the sky (within a SDSS spectroscopic fibre of 3" diameter) and clear spectroscopic signal from both galaxies at distinct redshifts.

In this paper, we present the blended spectra catalogue based on the Galaxy And Mass Assembly (GAMA) survey (Driver et al. 2009, 2011; Baldry et al. 2010) as candidates for either strong lensing follow-up or occulting galaxy analysis (e.g., HST imaging or spectroscopy). The GAMA data is an improvement over SDSS as the target galaxies can be fainter, the aperture is smaller (i.e., a closer overlap of the galaxies) and the AUTOZ detection algorithm is a marked improvement on the SDSS detections. The paper is organized as follows: §2 briefly introduces the GAMA survey, §3 the redshift determination and selection of blended spectra, §4 presents the visual classifications of the blended objects, §5 presents the blended spectra catalogue and we discuss the pair classification and their possible future uses in §6.

## 2 GALAXY AND MASS ASSEMBLY (GAMA) SURVEY

The GAMA survey has obtained over 250 000 galaxy redshifts selected to  $r < 19.8$  mag over  $290$  deg<sup>2</sup> of sky (Driver et al. 2009, 2011; Baldry et al. 2010; Liske 2015). At the heart of this survey is the redshift survey with the upgraded 2dF spectrograph AAOmega (Sharp et al. 2006; Saunders et al. 2006) on the Anglo-Australian Telescope. The GAMA survey extends over three equatorial survey regions of  $60$  deg<sup>2</sup> each (called G09, G12 and G15) and two Southern regions of similar area (G02, G23). See Baldry et al. (2010) for a detailed description of the GAMA input catalogue for the equatorial regions.

<sup>1</sup> The one exception is where we attempt to measure blue light attenuation. In this case, a spiral galaxy, which is brighter in the blue, is preferred.

The redshift survey in combination with a wealth of imaging data has led to many science results already. We use for this work the GAMA II redshifts (Liske 2015), which were obtained using a robust cross-correlation method for spectra with and without strong emission lines (Baldry et al. 2014).

### 3 SELECTION OF BLENDED SPECTRA

Galaxy redshifts were initially determined by a supervised fit (Liske 2015) but a recent upgrade to the GAMA survey pipeline includes a fully-automated template-based redshift determination (AUTOZ, Baldry et al. 2014). In certain cases, the fits for different templates resulted in two high-fidelity, but different redshifts; these are the candidate blended objects of interest to us here.

The AUTOZ code obtains cross-correlation redshifts against stellar and galaxy templates with varying strength of emission and absorption line features. The height and position of the first four peaks of normalized cross-correlation functions are obtained. These are called  $r_x$ ,  $r_{x,2}$ ,  $r_{x,3}$  and  $r_{x,4}$  each with a corresponding redshift and template number, with the peaks separated by at least 600 km/s. High values of  $r_x$  and  $r_{x,2}$ , particularly relative to  $r_{x,3}$  and  $r_{x,4}$ , can then be used to select candidate blended spectra.

The AUTOZ algorithm marks a significant improvement in the identification of blended spectra over that which could be obtained from GAMA I redshifts. In the initial redshift campaign, “redshifters” – the GAMA team members identifying the redshift with RUNZ – were focused on attaining a reliable redshift for single objects. In such an approach, only those spectra with wildly different redshifts by two redshifters or spectra remarked upon during visual inspection would be selected. With AUTOZ, blended spectra are identified as different redshifts using normalized cross-correlation functions, a much more objective and complete approach.

#### 3.1 AUTOZ selection

Double redshift selection using the AUTOZ approach was to require that two different redshifts had high cross-correlation peaks ( $r_x$  and  $r_{x,2}$ ), while the next two redshifts had significantly lower peak values. In order to address this, we defined the ratio between the second redshift peak value and subsequent, third and fourth, redshift peaks to be:

$$\mathcal{R} = r_{x,2} / \sqrt{(r_{x,3}^2 + r_{x,4}^2)} \quad (1)$$

To select the double- $z$  candidates, we required  $\mathcal{R} > 1.85$  (to avoid aliasing and a clean selection of real blends, see Figures 1 and 2) and for the first two redshifts to be from galaxy spectral templates. The galaxy spectral templates used in AUTOZ were from SDSS. An early version of the code used the SDSS DR2 templates, while a later version used templates derived from the Bolton et al. (2012) galaxy eigen-spectra. These later templates were numbered 40-47 in order of increasing emission-line strength. To broadly classify the templates, we select templates 40-42 as ‘passive galaxies’ (PG) and 43-47 as ‘emission-line galaxies’ (ELG).

Initially, we selected candidates with  $\mathcal{R} > 1.85$  and  $r_{x,2} > 5.5$ , with these values determined using the early

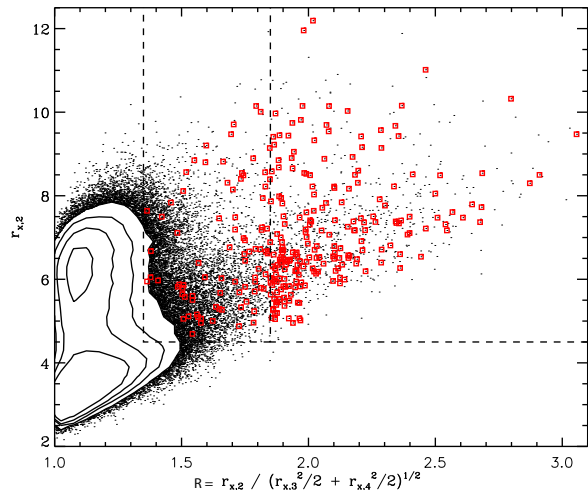


**Figure 1.** Distribution in selection parameters: for all GAMA spectra shown with contours and black points, and selected candidates shown with red squares. Note the all GAMA sample includes star-galaxy blends. The main selection criteria was  $\mathcal{R} > 1.85$  and this results in  $r_{x,2} > 4.5$  by default. Candidates from an earlier version of the code have  $\mathcal{R}$  between 1.35 and 1.85. These boundaries are shown with dashed lines.

version of the code. After the code was updated, the value of  $\mathcal{R}$  changed as a result of the new templates and a modest increase in the allowed redshift range from 0.8 to 0.9. Using the new values, we selected candidates with  $\mathcal{R} > 1.85$  and with no restriction on  $r_{x,2}$ . Old candidates were retained subject to a couple of criteria: the new value of  $\mathcal{R}$  was still greater than 1.35, and  $(1+z)/(1+z_2)$  was not near a problematic cross-correlation alias. Aliases can result from the matching of different emission lines in the templates to a strong line in the data. All candidates, old and new, near the alias of  $(1+z)/(1+z_2) = 1.343 \pm 0.002$  ( $\sim 5007/3727$ ) or the inverse were removed from the sample. Figure 1 shows the distribution of candidates in  $r_{x,2}$  versus  $\mathcal{R}$ , i.e. the selection parameters. Figure 2 shows where the aliases lie, in  $z_2$  versus  $z$ , with respect to the candidates.

The selection resulted in 280 galaxy pair candidates (from 299 blended spectra – some source locations were observed more than once). Depending on which template matched best for both redshifts in the blend, we classified the type of blends as follows: two passive-template galaxies (PG+PG), two emission-line templates (ELG+ELG), a passive template at low redshift and emission line template at higher redshift (PG+ELG), or vice versa (ELG+PG). Table 1 summarizes the resulting classifications. The AUTOZ results for our 280 blended objects are listed in Table 3.

### 4 VISUAL CLASSIFICATION

We visually classified all the 280 galaxy pairs identified by AUTOZ using the SDSS image viewer and GAMA cutouts in the case of the Southern fields. We classify whether the object appears as a single galaxy (either S or E, where S can mean a spiral galaxy or an irregular one i.e., late-type, except in a few clear cases and E an early type), an occulting pair or a disturbed ongoing merger (M). We sub-classify

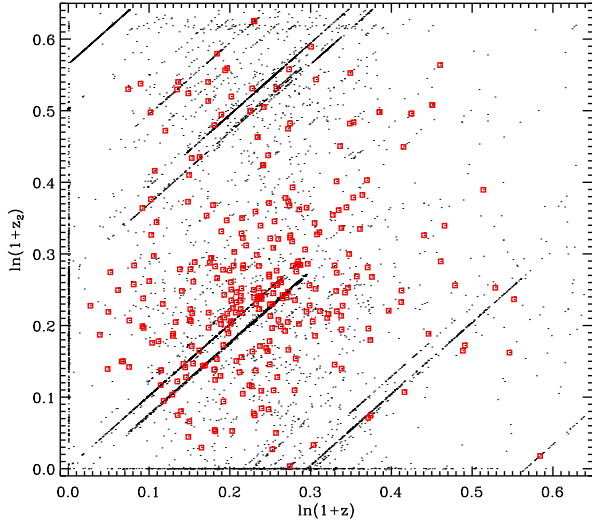


**Figure 2.** Distribution in  $z_2$  versus  $z$ : for all GAMA spectra with  $\mathcal{R} > 1.35$  and  $r_{x,2} > 4.5$  shown with black points, and for the selected candidates ( $\mathcal{R} > 1.85$ ) shown with red squares. Most candidates lie away from the alias lines that appear parallel when plotting the logarithm of one plus redshift on each axis.

**Table 1.** The numbers of different blended spectra identified in GAMA using the AUTOZ algorithm.

Pair Type	Number
ELG+ELG	78
ELG+PG	71
PG+ELG	104
PG+PG	27
Total	280

the occulting pair similar to the Keel et al. (2013) classification (Table 2) but given the limited image resolution the classification is essentially S-E, S-S or E-E. We introduce a sub-classification for single early types with some blue fuzzy hue on one side of the SDSS *gri* composite galaxy images (Ef). These latter could be lensing ellipticals or simply occulting pairs with a very small irregular galaxy in the foreground.

The classifications are listed in Table 2. Figure 3 shows the distribution of visual classifications of the blended spectrum objects. One would expect a reasonable correlation between the spectral typing (e.g., passive vs. emission-line) with the visual classifications, e.g., passive spectra dominating those pairs with an E type galaxy in the foreground. The relation between visual classification and spectral classification is tenuous. Visual classification based on color images can be both powerful but also misleading. Blue galaxies tend to be classified as late-types even if their profile is actually that of a spheroid.

With this in mind, two of us (BWH and AM) re-classified *sdss-i* postage stamps from the KiLO Degree Survey (KiDS) survey (de Jong et al. 2012). Figure 4 shows the distribution of these visual classifications. Because these are single-filter, the classification *Bf* is impossible. The new vi-

**Table 2.** The Keel et al. (2013) classification of the occulting galaxy pairs.

Classification	Description
F	spirals seen nearly face-on in front of an elliptical or S0 background system.
Q	the background galaxy is nearly edge-on and is projected nearly radial.
$\Phi$	the spiral is seen essentially edge-on, at least partially backlit by a smooth galaxy.
X	two edge-on disk galaxies
SE	Spiral in front of an Elliptical, not in one of the above categories.
S	spiral/spiral overlaps.
B	the background galaxy has much smaller angular size than the foreground disk.
E	pairs containing only elliptical or S0 galaxies.

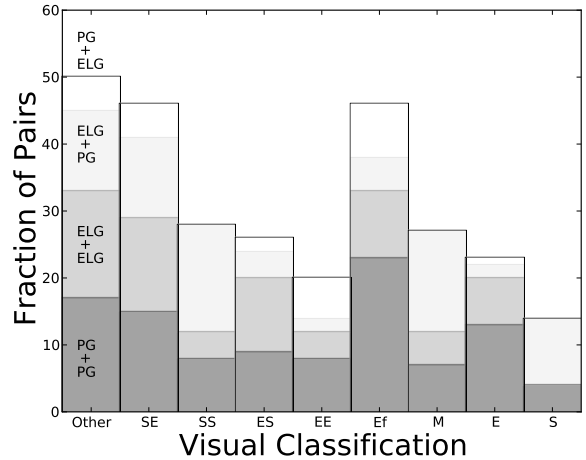


**Figure 3.** The distribution of visual classifications for all the blended spectra broken down into all four possible template combinations (PG=passive template, ELG=emission line template, PG+ELG is a passive in front of an emission line pair). No clear correlation between the SDSS visual classifications and the template ones is evident. The "other" category are objects without SDSS imaging or a reasonable classification.

sual classifications remains poorly correlated with the spectral classification.

In our opinion, both the SDSS color-images or the deeper and higher resolution KiDS single-filter images are still too low-resolution to unambiguously disentangle and visually classify these objects. These objects are inherently blended ones. Even with another improvement in spatial resolution (i.e., HST imaging), visual classifications will remain subjective –although it is encouraging that BWH and AM agreed on the visual classifications. And it remains difficult to ascertain which object is in the foreground in a visual classification.

**Table 3.** The complete catalogue of blended spectra in the GAMA survey. T1 and T2 refer to the template numbers for the first and second peaks. The full catalog is available in the appendix.

Field	GAMA-id	RA	DEC	$z$	T1	$r_x$	$z_2$	T2	$r_{x,2}$	Spec. Type	Vis. Type
G09	196060	129.01621	-0.69336	0.293	40	8.7	0.051	46	5.6	ELG+PG	SE
G09	197073	133.78179	-0.74790	0.270	40	10.8	0.268	44	6.4	ELG+PG	EE
G09	198082	138.28150	-0.66673	0.163	40	11.1	0.321	47	10.2	PG+ELG	ES
G09	202448	129.69546	-0.38179	0.418	40	9.0	0.738	45	5.0	PG+ELG	SE
G09	204140	136.63883	-0.35203	0.282	40	9.4	0.449	47	8.1	PG+ELG	Ef
G09	209222	132.36771	0.16360	0.128	40	10.3	0.603	47	6.7	PG+ELG	E
G09	209263	132.50596	0.04250	0.310	42	6.5	0.270	46	5.3	ELG+PG	Ef
G09	209295	132.61013	0.11972	0.313	40	11.2	0.608	47	7.8	PG+ELG	Ef
...	...	...	...	...	...	...	...	...	...	...	...

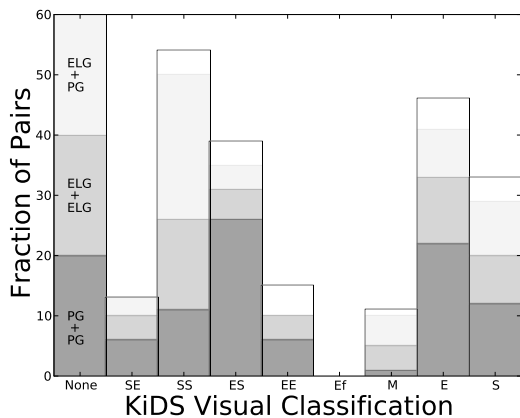


**Figure 4.** The distribution of visual classifications of the KiDS *sdss-i* filter for all the blended spectra broken down into all four possible template combinations (PG=passive template, ELG=emission line template, PG+ELG is a passive in front of an emission line pair). The lack of a correlation between visual and spectral classification persist with the single-filter classifications.

## 5 CATALOG

We have classified the blended spectra by the best-fit templates (PG=passive template, ELG=emission line template) denoting them with Foreground+Background best fit template. Out of 280 galaxies, we identify: 104 lens candidates, passive galaxies with emission-line galaxies at higher redshifts (PG+ELG); 71 ideal occulting galaxy pairs, emission-line galaxies in front of a passive galaxies (ELG+PG); 78 occulting pairs with both foreground and background galaxies showing strong emission lines, ELG+ELG; and 27 double passive occulting pairs (PG+PG), with both galaxies having passive template fits (Table 1). Figure 5 shows the distribution of foreground and background galaxy best-fit templates. We characterize PG+ELG pairs as possible lensing pairs as this is how the SLACS survey found the majority of their strong gravitational lensing pairs, confirmed with HST imaging (Treu et al. 2006; Koopmans et al. 2006; Gavazzi et al. 2007; Bolton et al. 2008a; Gavazzi et al. 2008; Bolton et al. 2008b; Treu et al. 2009). There is a preference for template 40 in the case of foreground galaxies. We interpret this as a selection effect: it is easier to identify anomalous emis-

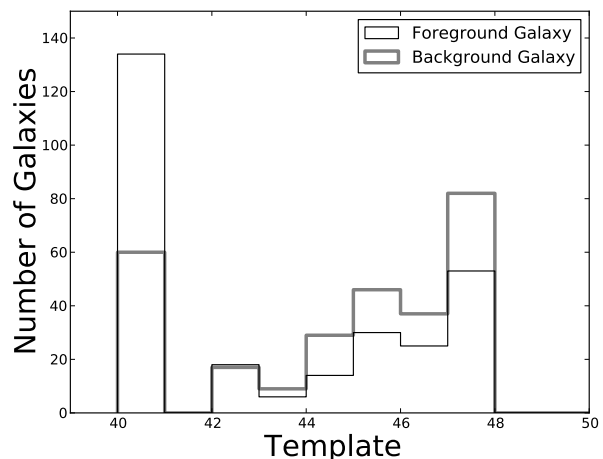
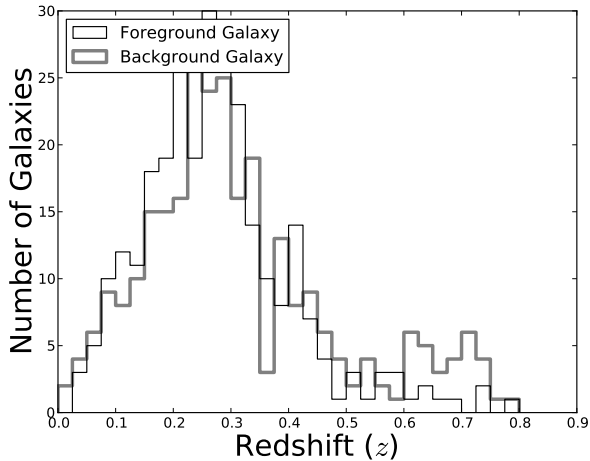


**Figure 5.** The distribution of GAMA spectroscopic best template for the blended spectra catalogue. The templates are numbered from 40–47 in order of increasing emission-line strength. To broadly classify the templates, we select templates 40–42 as “passive galaxies” (PG) and 43–47 as “emission-line galaxies” (ELG).

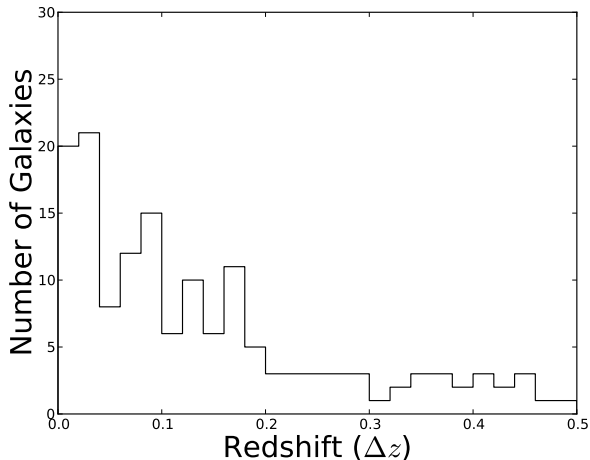
sion lines on top of a passive spectrum (template 40 has the weakest emission lines). Apart from the preference for template 40 for foreground objects, the distribution is relatively similar. The AUTOZ classification is not particularly biased against either combination of spectra in a blend.

Figure 6 shows the distribution of redshifts for both the foreground and background galaxies in the blended spectra. Background galaxy redshifts peak around  $z = 0.3$  and foreground galaxies a little below that. Similar to the redshift completeness of the GAMA survey (Baldry et al. 2014; Liske 2015), the sample is complete for  $z < 0.4$  regardless of template but objects can still be detected out to  $z < 0.8$ , beyond which the AUTOZ are limited because of a lack of information in the GAMA spectra. The pair members are typically well separated in redshift ( $\Delta z > 600 \text{ km/s}$ ). Figure 7 shows the redshift difference for the blended spectra, making these ideal pairs for either lensing studies or as occulting galaxies.

To classify the pairs into strong lens candidates (PG+ELG) and ELG+PG, ELG+ELG, and PG+PG occulting pairs, we employ the best template fits. Lenses (PG+ELG) are difficult to verify from ground-based imaging, but Arneson et al. (2012) argue that spectroscopic se-



**Figure 6.** The distribution of GAMA spectroscopic redshifts for the blended spectra catalogue. AUTOZ excludes redshift candidates within 600 km/s of another redshift by design.



**Figure 7.** The difference in redshift between the foreground and background galaxies in blended spectra catalogue.

lection of lenses are both complete and relatively unbiased within the Einstein ring. Therefore the list of lenses presented here, especially those in the G23 field (not covered by SDSS), are new candidates for possible HST follow-up. Figure 9 shows some random examples of “ideal” occulting pairs (ELG+PG). In Holwerda et al. (2007b), we found that 86 out of 101 candidate from SLACS were usable occulting pairs. Figure 9 shows that indeed most of the spectroscopically-identified occulting pairs have a good geometry to extract, in principle, the transmission of the foreground galaxies. These new pairs will be of use to model the transmission of the foreground galaxy with a very low impact parameter (almost perfectly aligned galaxies). Alternate occulting galaxy pairs are the ELG+ELG type, which can be used to extract transmission though the foreground galaxy in the bluer wavelengths. For example, Keel et al. (2014) use such spiral-spiral pairs to infer the extinction

law in the ultraviolet. This can only be done with a UV-bright spiral as the background galaxy. Intrinsic asymmetry in spiral structure of both pair members introduces uncertainty in the transmission/opacity measurement, but does not introduce a bias. However, irregular galaxies cannot be used as background illuminators. The ELG+ELG occulters are therefore a useful sub-sample of the occulting pairs. Certainly, one is a clear ELG+ELG pair but many other include an irregular as well. Lastly, we have PG+PG pairs, where both galaxies lack emission lines. These may be lenses still, but are unlikely to attract follow-up attention. As occulting galaxies they are not likely to reveal much new information about the dusty ISM in early-types.

## 6 CONCLUDING REMARKS

From the  $\sim 230\,000$  objects with spectroscopy in the GAMA survey, we identified 280 blended objects ( $\sim 0.12\%$ ). In contrast, out of the 849 920 spectra in SDSS/DR4 (Adelman-McCarthy et al. 2006), Bolton et al. (2008a) identified a total of 89 lenses and Holwerda et al. (2007b) identified 101 candidate occulting galaxy pairs, i.e., 0.02% of all the SDSS spectra were blends. To make an honest comparison, we can only count the early-type, passive spectra with emission line at different redshift, the target of Bolton et al. (2004) and the subsequent SLACS survey. In GAMA, we identify  $104+71=179$  of these (0.08%), a factor four higher detection rate.

There are obvious differences between the SDSS and GAMA redshift surveys: a fainter limiting magnitude and a higher completeness (by design) for the GAMA survey. The fainter depth by two magnitudes means that there are about ten times as many galaxies with a similar magnitude (e.g.,  $r \sim 19.5$  for GAMA,  $r \sim 17.5$  for SDSS main galaxy sample). This will result in more blended spectra despite the fact the AAOmega apertures are  $2''$  compared to  $3''$  for SDSS. This latter difference diminishes the GAMA survey’s sensitivity to overlapping pairs; a wider aperture includes more flux from the outskirts of the occulting galaxy. Naively, one would therefore expect a factor  $\sim 4.5$  improvement in sensitivity of GAMA with respect to SDSS for blended spectra, which bears out approximately (0.12% of GAMA vs. 0.02% of SDSS/DR4), better than the increase in blended spectra from SDSS DR4 to DR10. Another difference between the surveys is the identification of the redshift blend. In the SLACS survey, potentially lensed star-forming galaxies are detected through the presence of background oxygen and hydrogen nebular emission lines in the SDSS-DR4 spectra of massive foreground galaxies. The GAMA identification, this paper, is through a complete-spectrum cross-correlation with different templates, which uses the full spectral range to identify redshift, and allows for two blended passive spectra or at least does not require very strong emission lines at different redshifts.

There are several possible uses for these blended spectral galaxy pairs.

The occulting pairs in GAMA are added to the master occulting galaxy catalogue, predominantly based on the SDSS spectral identifications (86 blended pairs in Holwerda et al. 2007b), and the GalaxyZoo identifications (1993, Keel et al. 2013).

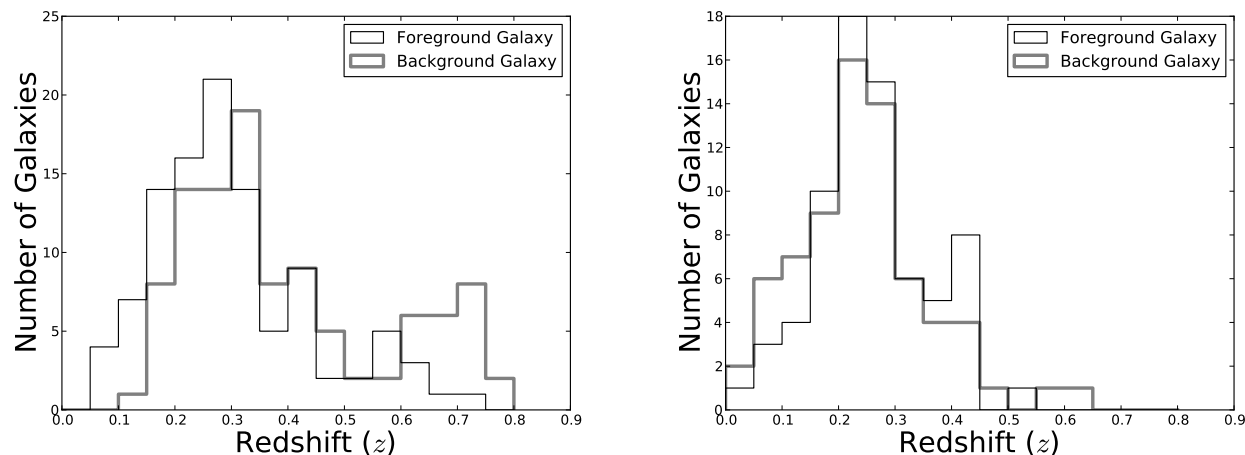


**Figure 8.** The distribution of foreground galaxy redshift and background galaxy redshift for the passive foreground with emission-line background templates (PG+ELG, left panel) and the emission-line foreground template with a passive template for the background objects (ELG+PG, right).

The presented catalogue of occulting pairs constitutes one way to identify occulting pairs in GAMA. Another approach uses the rejects from the pairs and group catalogue: galaxy pairs that are close on the sky but separated enough to warrant separate fibre assignment and do not exhibit a blended spectrum. By requiring that both pair members are well-separated in redshift, we obtain bona-fide occulting pairs.

A complete catalogue of galaxy groups is one of the primary goals of the GAMA survey (Robotham et al. 2011, 2014). A second sample of overlapping pairs will be identified from this catalogue, once it is complete ( $\sim 300$  expected). Therefore, between the high-fidelity automated identification of shared-fibre pairs and simultaneously, a complete census of close, serendipitous overlaps with separate redshifts, the GAMA identifications of overlapping galaxies will be the most complete to date.

In the case of the lenses, the presented lensing galaxy candidates represent a near doubling of the known objects from SLACS (89 lenses) and a useful addition to the BOSS identified ones (Bolton et al. 2012). The increased depth and completeness of GAMA means more distant and lower mass lenses are included. It should be illustrative to study these blended objects with the ongoing IFU surveys (e.g., SAMI or MANGA) and perhaps spatially separate the blended spectral signal or at least study the variation with fibre of the blended signal. For a full lensing analysis, the imaging will have to be higher spatial resolution than those available from either SDSS, KiDS or any of the other imaging surveys available for GAMA. Either dedicated VLT/AO observations or HST imaging would fit the bill. The benefits of the GAMA selection are lower-mass lenses and lensed images closer to the lensing galaxy.

## ACKNOWLEDGEMENTS

The authors thank the referee for his or her comments and suggestions. The lead author thanks the European Space

Agency for the support of the Research Fellowship program and the whole GAMA team for a magnificent observational effort. GAMA is a joint European-Australasian project based around a spectroscopic campaign using the Anglo-Australian Telescope. The GAMA input catalogue is based on data taken from the Sloan Digital Sky Survey and the UKIRT Infrared Deep Sky Survey. Complementary imaging of the GAMA regions is being obtained by a number of independent survey programs including GALEX MIS, VST KiDS, VISTA VIKING, WISE, Herschel-ATLAS, GMRT and ASKAP providing UV to radio coverage. GAMA is funded by the STFC (UK), the ARC (Australia), the AAO, and the participating institutions. The GAMA website is [www.gamasurvey.org/](http://www.gamasurvey.org/). MJIB acknowledges financial support from the Australian Research Council (FT100100280) This research has made use of the NASA/IPAC Extragalactic Database (NED) which is operated by the Jet Propulsion Laboratory, California Institute of Technology, under contract with the National Aeronautics and Space Administration. This research has made use of NASA’s Astrophysics Data System.

## REFERENCES

- Adelman-McCarthy J. K. et al., 2006, *ApJS*, 162, 38
- Albrecht A. et al., 2006, *astro-ph/0609591*
- Andredakis Y. C., van der Kruit P. C., 1992, *A&A*, 265, 396
- Arneson R. A., Brownstein J. R., Bolton A. S., 2012, *ApJ*, 753, 4
- Baes M. et al., 2010, *A&A*, 518, L39+
- Baldry I. K. et al., 2014, *MNRAS*, 441, 2440
- Baldry I. K. et al., 2010, *MNRAS*, 404, 86
- Bendo G. J. et al., 2014, *ArXiv e-prints*
- Bendo G. J. et al., 2012, *MNRAS*, 419, 1833
- Berlind A. A., Quillen A. C., Pogge R. W., Sellgren K., 1997, *AJ*, 114, 107
- Bianchi S., Xilouris E. M., 2011, *A&A*, 531, L11+

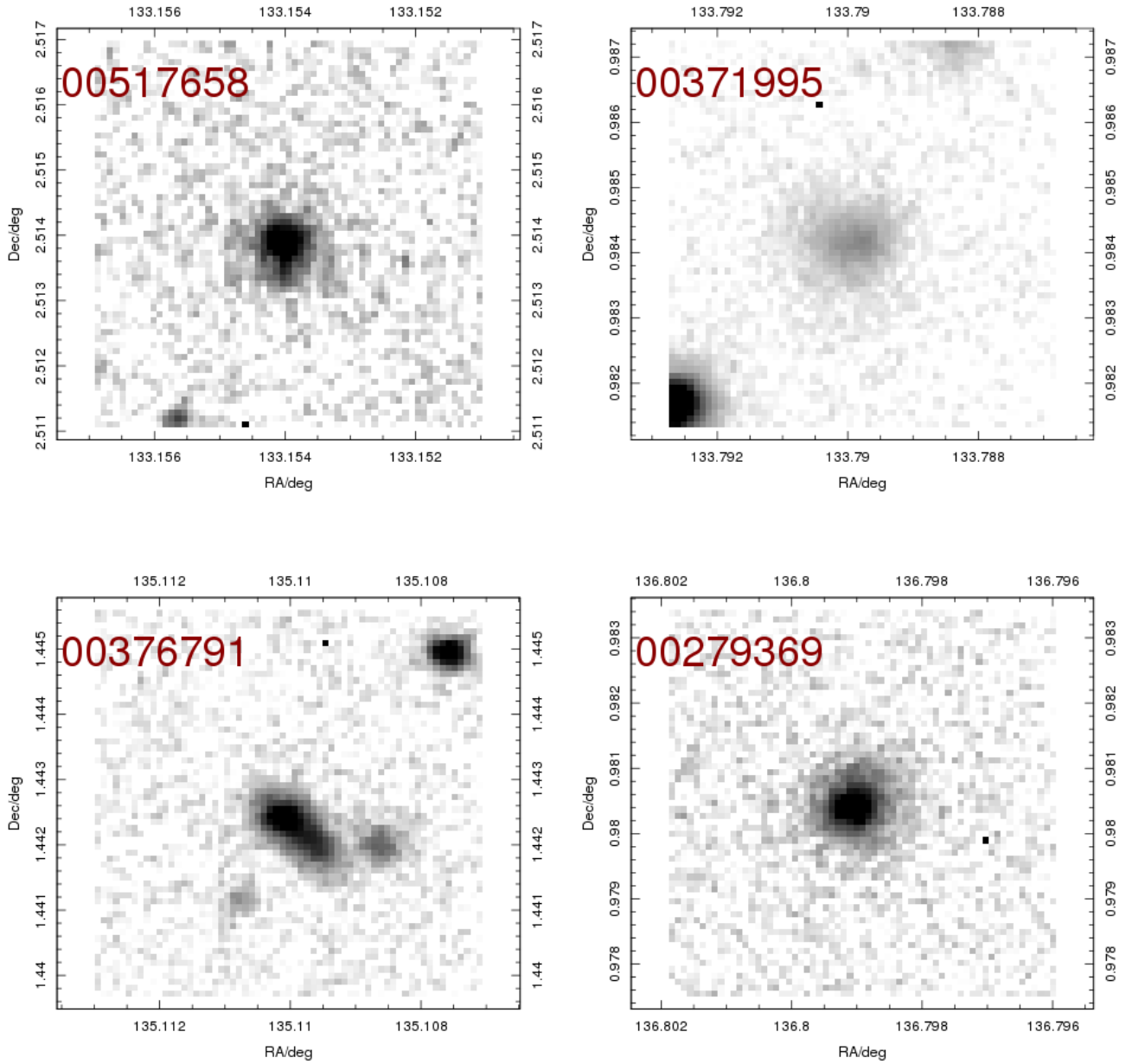


**Figure 9.** Examples of the ELG+PG pairs. SDSS-i image cutouts retrieved using <http://ict.icrar.org/cutout/>. Standard cutout size is 20". GAMA id numbers are in red.

Bolton A. S. et al., 2012, *ApJ*, 757, 82

Bolton A. S., Burles S., Koopmans L. V. E., Treu T., Gavazzi R., Moustakas L. A., Wayth R., Schlegel D. J., 2008a, *ApJ*, 682, 964

Bolton A. S., Burles S., Koopmans L. V. E., Treu T., Moustakas L. A., 2006, *ApJ*, 638, 703

Bolton A. S., Burles S., Schlegel D. J., Eisenstein D. J., Brinkmann J., 2004, *AJ*, 127, 1860

Bolton A. S., Treu T., Koopmans L. V. E., Gavazzi R., Moustakas L. A., Burles S., Schlegel D. J., Wayth R., 2008b, *ApJ*, 684, 248

Brownstein J. R. et al., 2012, *ApJ*, 744, 41

Cuillandre J., Lequeux J., Allen R. J., Mellier Y., Bertin E., 2001, *ApJ*, 554, 190

de Jong J. T. A., Verdoes Kleijn G. A., Kuijken K. H., Valentijn E. A., KiDS, consortiums A.-W., 2012, *ArXiv e-prints*

de Looze I. et al., 2012, *MNRAS*, 427, 2797

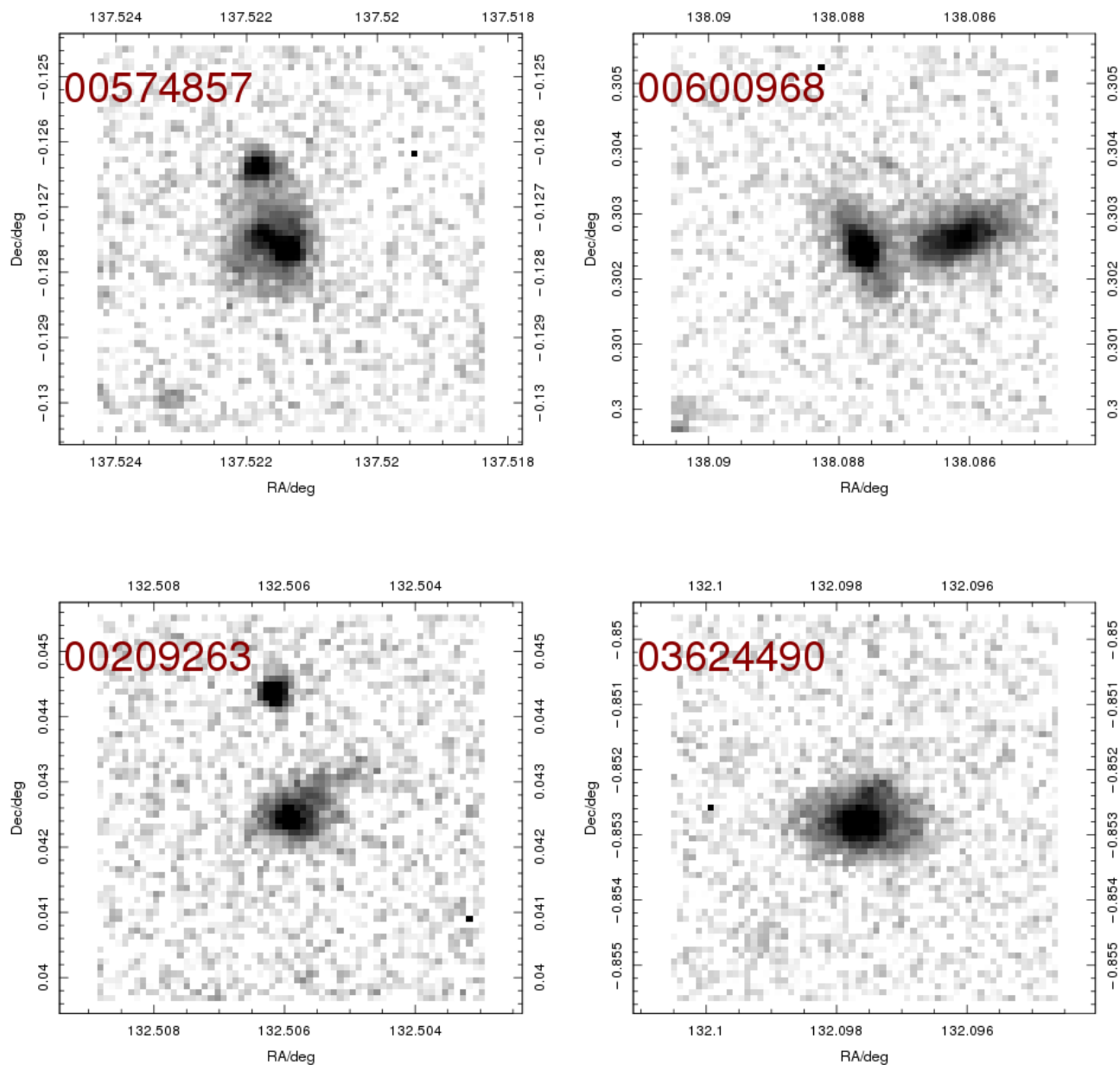
Domingue D. L., Keel W. C., Ryder S. D., White, III R. E., 1999, *AJ*, 118, 1542

Domingue D. L., Keel W. C., White, III R. E., 2000, *ApJ*, 545, 171

Draine B. T. et al., 2014, *ApJ*, 780, 172

Driver S. P. et al., 2011, *MNRAS*, 413, 971



Figure 9. – *continued*

Driver S. P. et al., 2009, *Astronomy and Geophysics*, 50, 050000

Elmegreen D. M., Kaufman M., Elmegreen B. G., Brinks E., Struck C., Klarić M., Thomasson M., 2001, *AJ*, 121, 182

Galametz M. et al., 2012, *MNRAS*, 425, 763

Gavazzi R., Treu T., Koopmans L. V. E., Bolton A. S., Moustakas L. A., Burles S., Marshall P. J., 2008, *ApJ*, 677, 1046

Gavazzi R., Treu T., Rhodes J. D., Koopmans L. V. E., Bolton A. S., Burles S., Massey R. J., Moustakas L. A., 2007, *ApJ*, 667, 176

González R. A., Allen R. J., Dirsch B., Ferguson H. C.,

Calzetti D., Panagia N., 1998, *ApJ*, 506, 152

González R. A., Loinard L., Allen R. J., Muller S., 2003, *AJ*, 125, 1182

Hinz J. L. et al., 2012, *ApJ*, 756, 75

Hinz J. L., Engelbracht C. W., Willmer C. N. A., Rieke G. H., Rieke M. J., Smith P. S., Blaylock M., Gordon K. D., 2009, in *The Evolving ISM in the Milky Way and Nearby Galaxies*

Holwerda B. W., 2005, PhD thesis, Proefschrift, Rijksuniversiteit Groningen, 2005

Holwerda B. W., 2008, *MNRAS*, 386, 475

Holwerda B. W., Allen R. J., de Blok W. J. G., Bouchard A., Gonzalez-Lopezlira R. A., van der Kruit P. C., Leroy

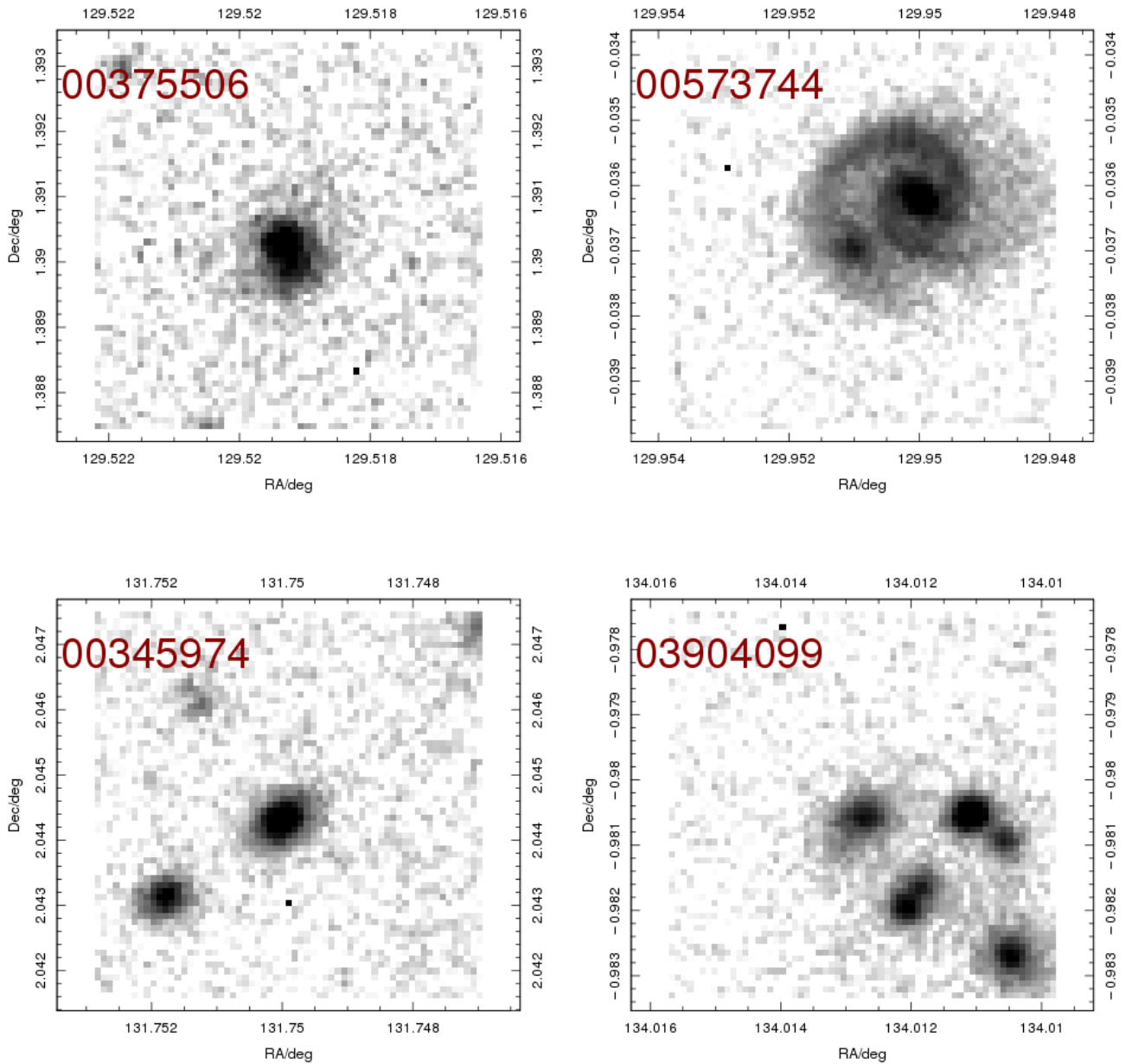


**Figure 10.** Examples of the ELG+ELG pairs. SDSS-i image cutouts retrieved using <http://ict.icrar.org/cutout/>. Standard cutout size is  $20''$ . GAMA id numbers are in red. Emission line galaxies include irregulars which limit the use of this class of objects in follow-up analysis.

A., 2012a, ArXiv e-prints

Holwerda B. W. et al., 2012b, *A&A*, 541, L5

Holwerda B. W., Böker T., Dalcanton J. J., Keel W. C., de Jong R. S., 2013, *MNRAS*, 433, 47

Holwerda B. W. et al., 2007a, *AJ*, 134, 2226

Holwerda B. W., González R. A., Allen R. J., van der Kruit P. C., 2005a, *AJ*, 129, 1381

Holwerda B. W., González R. A., Allen R. J., van der Kruit P. C., 2005b, *AJ*, 129, 1396

Holwerda B. W., González R. A., Allen R. J., van der Kruit P. C., 2005c, *A&A*, 444, 101

Holwerda B. W., González R. A., Allen R. J., van der Kruit P. C., 2005d, *A&A*, 444, 319

Holwerda B. W., González R. A., van der Kruit P. C., Allen R. J., 2005e, *A&A*, 444, 109

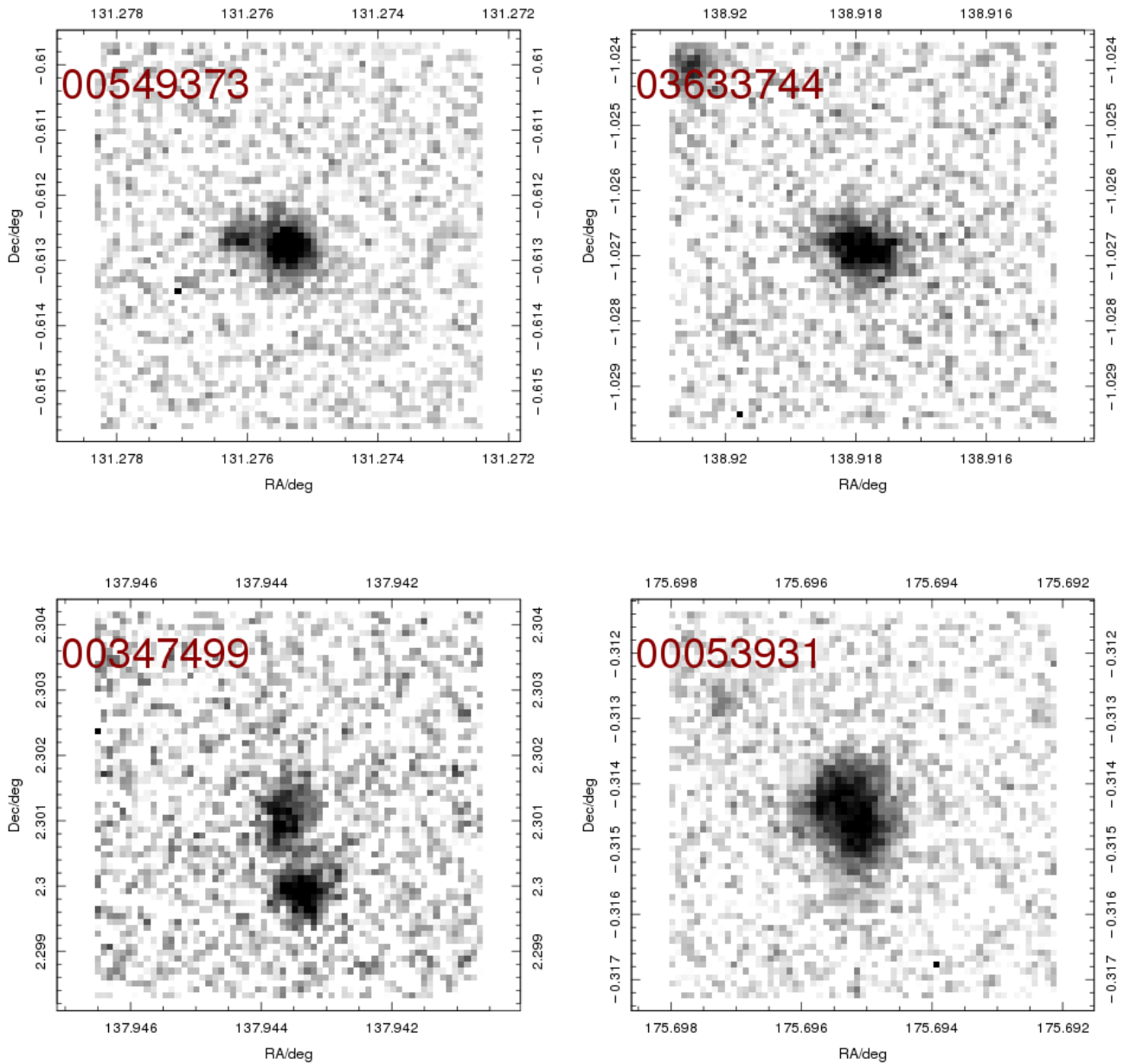
Holwerda B. W., Keel W. C., 2013, *A&A*, 556, A42

Holwerda B. W., Keel W. C., Bolton A., 2007b, *AJ*, 134, 2385

Holwerda B. W., Keel W. C., Williams B., Dalcanton J. J., de Jong R. S., 2009, *AJ*, 137, 3000

Holwerda B. W. et al., 2007c, *AJ*, 134, 1655

Holwerda B. W., Reynolds A., Smith M., Kraan-Korteweg

Figure 10. – *continued*

R. C., 2014, ArXiv e-prints

Hughes T. M. et al., 2014a, *A&A*, 565, A4

Hughes T. M. et al., 2014b, ArXiv e-prints

Keel W. C., Manning A. M., Holwerda B. W., Lintott C. J., Schawinski K., 2014, *AJ*, 147, 44

Keel W. C., Manning A. M., Holwerda B. W., Mezzoprete M., Lintott C. J., Schawinski K., Gay P., Masters K. L., 2013, *PASP*, 125, 2

Keel W. C., White, III R. E., 2001a, *AJ*, 121, 1442

Keel W. C., White, III R. E., 2001b, *AJ*, 122, 1369

Koopmans L. V. E., Treu T., Bolton A. S., Burles S., Moustakas L. A., 2006, *ApJ*, 649, 599

Lintott C. J. et al., 2008, *MNRAS*, 389, 1179

Liske J. e. a., 2015, *MNRAS*, submitted

Popescu C. C., Misiriotis A., Kyllafis N. D., Tuffs R. J., Fischera J., 2000, *A&A*, 362, 138

Popescu C. C., Tuffs R. J., Dopita M. A., Fischera J., Kyllafis N. D., Madore B. F., 2011, *A&A*, 527, A109+

Robotham A. S. G. et al., 2014, *MNRAS*, 444, 3986

Robotham A. S. G. et al., 2011, *MNRAS*, 416, 2640

Saunders A., Goldman D. I., Full R. J., Buehler M., 2006, in *Society of Photo-Optical Instrumentation Engineers (SPIE) Conference Series*, Vol. 6230, *Society of Photo-Optical Instrumentation Engineers (SPIE) Conference Series*, p. 17

Sharp R. et al., 2006, in *Society of Photo-Optical In-*

- strumentation Engineers (SPIE) Conference Series, Vol. 6269, Society of Photo-Optical Instrumentation Engineers (SPIE) Conference Series
- Smith M. W. L. et al., 2010, *A&A*, 518, L51+
- Treu T., Gavazzi R., Gorecki A., Marshall P. J., Koopmans L. V. E., Bolton A. S., Moustakas L. A., Burles S., 2009, *ApJ*, 690, 670
- Treu T., Koopmans L. V., Bolton A. S., Burles S., Moustakas L. A., 2006, *ApJ*, 640, 662
- Verstappen J. et al., 2013, *A&A*, 556, A54
- White R. E., Keel W. C., 1992, *Nature*, 359, 129
- White, III R. E., Keel W. C., Conselice C. J., 2000, *ApJ*, 542, 761
- Xilouris E. M. et al., 2012, *A&A*, 543, A74

**Table 4.** The complete catalogue of blended spectra in the GAMA survey (online in MNRAS). T1 and T2 refer to the template numbers for the first and second peaks.

Field	GAMA-id	RA	DEC	$z$	T1	$r_x$	$z_2$	T2	$r_{x,2}$	Spec. Type	Vis. Type
G09	196060	129.01621	-0.69336	0.293	40	8.7	0.051	46	5.6	ELG+PG	SE
G09	197073	133.78179	-0.74790	0.270	40	10.8	0.268	44	6.4	ELG+PG	EE
G09	198082	138.28150	-0.66673	0.163	40	11.1	0.321	47	10.2	PG+ELG	ES
G09	202448	129.69546	-0.38179	0.418	40	9.0	0.738	45	5.0	PG+ELG	SE
G09	204140	136.63883	-0.35203	0.282	40	9.4	0.449	47	8.1	PG+ELG	Ef
G09	209222	132.36771	0.16360	0.128	40	10.3	0.603	47	6.7	PG+ELG	E
G09	209263	132.50596	0.04250	0.310	42	6.5	0.270	46	5.3	ELG+PG	Ef
G09	209295	132.61013	0.11972	0.313	40	11.2	0.608	47	7.8	PG+ELG	Ef
G09	209584	134.02979	0.15244	0.167	46	12.0	0.158	40	7.9	PG+ELG	SE
G09	218757	140.75621	0.84809	0.238	47	9.9	0.250	44	9.1	ELG+ELG	Ef
G09	279369	136.79904	0.98044	0.284	40	8.5	0.238	46	7.2	ELG+PG	ES/Ef
G09	279956	140.14187	0.97341	0.586	47	6.0	0.336	40	5.9	PG+ELG	ES
G09	300500	129.87425	1.12844	0.153	44	9.5	0.158	40	7.4	ELG+PG	SS/Q
G09	300979	131.46746	1.19884	0.146	40	6.8	0.716	40	5.8	PG+PG	SE
G09	301818	135.32929	1.22984	0.487	47	10.6	0.247	40	10.0	PG+ELG	SE/M
G09	302123	136.46358	1.31167	0.470	40	6.7	0.646	40	6.3	PG+PG	E
G09	302719	138.94058	1.33144	0.593	47	6.5	0.404	42	6.4	PG+ELG	SS
G09	323200	130.73717	1.55957	0.416	47	9.7	0.350	40	6.7	PG+ELG	EE
G09	323247	131.02333	1.64814	0.164	40	10.6	0.229	46	8.5	PG+ELG	SE
G09	324470	136.07796	1.68015	0.148	45	10.3	0.321	42	8.9	ELG+PG	SE/Phi
G09	325026	138.25700	1.72137	0.329	40	7.1	0.336	45	6.3	PG+ELG	ES/Ef
G09	325108	138.62475	1.87141	0.202	46	9.1	0.165	40	7.0	PG+ELG	Ef
G09	345974	131.75004	2.04437	0.207	46	11.2	0.231	45	8.5	ELG+ELG	Ef
G09	345984	131.78108	2.12672	0.207	40	8.1	0.138	46	7.6	ELG+PG	ES
G09	347499	137.94367	2.30107	0.316	45	8.9	0.381	47	5.9	ELG+ELG	SS
G09	348065	140.09571	2.33430	0.281	45	9.9	0.086	45	9.4	ELG+ELG	SS/M
G09	348299	140.94438	2.24256	0.409	42	10.4	0.279	45	6.3	ELG+PG	SE
G09	371208	130.50925	1.02071	0.077	40	7.7	0.699	46	6.0	PG+ELG	SS
G09	371995	133.78987	0.98418	0.108	47	8.6	0.386	42	7.9	ELG+PG	M
G09	372810	137.79708	1.07694	0.301	40	8.9	0.220	45	6.4	ELG+PG	ES
G09	375506	129.51933	1.39028	0.240	46	13.5	0.419	46	7.5	ELG+ELG	SE/F
G09	376767	134.88888	1.50709	0.727	47	7.4	0.176	46	6.7	ELG+ELG	SS
G09	376791	135.11008	1.44247	0.198	40	10.4	0.149	46	9.1	ELG+PG	ES/M
G09	377212	136.80625	1.64392	0.283	40	12.3	0.308	44	5.6	PG+ELG	EE/M
G09	377486	137.90642	1.62916	0.169	40	10.7	0.334	46	5.0	PG+ELG	E
G09	380839	130.27629	1.72911	0.361	42	8.4	0.387	47	7.3	PG+ELG	EE
G09	382083	135.24921	1.89325	0.098	47	8.5	0.217	40	7.1	ELG+PG	ES/M
G09	382857	138.76350	2.04159	0.341	40	6.1	0.358	46	4.9	PG+ELG	ES
G09	383053	139.68454	1.98081	0.189	45	9.0	0.671	47	7.6	ELG+ELG	S
G09	383284	140.65750	2.13736	0.194	40	9.7	0.342	47	5.8	PG+ELG	ES
G09	386427	132.24292	2.24817	0.209	42	7.5	0.393	40	6.6	PG+PG	EE
G09	387615	137.19829	2.40849	0.281	40	10.5	0.549	42	5.1	PG+PG	E/Ef
G09	388201	138.99892	2.51429	0.167	40	10.0	0.299	44	8.2	PG+ELG	ES
G09	417645	132.51888	2.29438	0.108	40	12.4	0.457	45	5.8	PG+ELG	S
G09	417922	134.09700	2.49636	0.198	40	9.1	0.615	42	6.5	PG+PG	Ef
G09	419678	140.98671	2.86084	0.569	40	8.2	0.662	47	7.4	PG+ELG	E
G09	422882	132.81062	2.83784	0.308	45	9.4	0.212	40	7.8	PG+ELG	SS
G09	425637	129.15721	2.86991	0.511	42	8.0	0.282	40	6.1	PG+PG	Ef
G09	528021	140.98654	-0.87061	0.157	40	9.1	0.136	44	6.7	ELG+PG	ES/Ef
G09	573657	129.41362	-0.01039	0.274	40	7.2	0.657	46	6.8	PG+ELG	E
G09	573744	129.95100	-0.03694	0.144	45	11.5	0.130	45	9.2	ELG+ELG	SE/B
G09	574390	135.66788	-0.13742	0.223	40	11.6	0.229	46	5.5	PG+ELG	X
G09	574857	137.52142	-0.12759	0.105	45	12.1	0.300	44	9.4	ELG+ELG	M/SS
G09	575653	140.77658	-0.11463	0.320	40	11.0	0.481	47	6.1	PG+ELG	Ef
G09	599598	132.08975	0.21503	0.118	45	6.4	0.195	40	5.8	ELG+PG	SE
G09	599770	132.67583	0.34792	0.191	40	7.7	0.333	40	7.6	PG+PG	SE
G09	599797	132.62096	0.25907	0.200	40	9.3	0.054	45	7.9	ELG+PG	Ef
G09	599995	133.35229	0.32283	0.289	43	9.1	0.292	43	5.6	ELG+ELG	E
G09	600968	138.08767	0.30248	0.053	46	10.9	0.316	42	8.2	ELG+PG	SE/Phi
G09	621991	129.85479	0.68659	0.145	40	7.2	0.078	45	5.8	ELG+PG	SE
G09	622326	132.66296	0.63611	0.378	42	7.5	0.234	40	7.1	PG+PG	EE/Ef

**Table 4.** – *continued.*

Field	GAMA-id	RA	DEC	$z$	T1	$r_x$	$z_2$	T2	$r_{x,2}$	Spec. Type	Vis. Type
G09	641911	140.01479	-1.21574	0.096	46	9.9	0.220	45	9.1	ELG+ELG	SE
G09	663372	140.42683	-1.09201	0.331	45	6.6	0.224	40	6.4	PG+ELG	Ef
G09	905359	139.63437	-0.60728	0.585	40	6.5	0.757	47	6.2	PG+ELG	E
G09	3576902	129.95892	-1.63319	0.268	45	9.7	0.187	40	7.3	PG+ELG	M
G09	3579777	131.41271	-1.66217	0.258	40	7.9	0.869	42	5.3	PG+PG	Ef
G09	3612009	135.81950	-1.34174	0.313	46	7.2	0.452	40	6.1	ELG+PG	M
G09	3624490	132.09767	-0.85274	0.366	40	8.3	0.246	46	7.4	ELG+PG	M/Ef
G09	3626956	134.23367	-0.80412	0.736	47	6.6	0.267	42	6.5	PG+ELG	Ef
G09	3632403	138.10708	-0.95852	0.315	40	10.1	0.444	47	8.5	PG+ELG	Ef
G09	3633744	138.91800	-1.02683	0.343	45	7.4	0.440	46	5.1	ELG+ELG	ES
G09	3866435	136.82975	-1.99357	0.325	47	9.3	0.166	44	8.5	ELG+ELG	S
G09	3884455	135.10842	-1.60189	0.411	42	9.2	0.440	47	7.4	PG+ELG	Ef
G09	3886423	136.26788	-1.56631	0.224	47	13.5	0.284	40	7.2	ELG+PG	ES
G09	3887215	136.64988	-1.59199	0.328	46	7.0	0.331	47	6.3	ELG+ELG	SS
G09	3890035	138.55021	-1.68663	0.259	40	9.1	0.868	42	6.0	PG+PG	Ef
G09	3904099	134.01279	-0.98051	0.217	46	11.5	0.242	47	6.5	ELG+ELG	SE
G09	3909630	137.37821	-1.17997	0.227	40	10.2	0.328	44	8.2	PG+ELG	SS/M
G09	3913313	139.74904	-1.30614	0.223	46	11.1	0.226	40	10.3	ELG+PG	E
G12	7242	176.29229	0.73915	0.529	40	8.3	0.642	47	8.2	PG+ELG	E
G12	7907	179.68421	0.82128	0.230	46	9.1	0.244	40	8.1	ELG+PG	SE
G12	9156	185.08025	0.71944	0.270	40	10.1	0.115	46	8.9	ELG+PG	ES
G12	22278	176.96358	1.20310	0.094	40	8.5	0.712	47	6.0	PG+ELG	S
G12	22559	178.05237	1.05246	0.283	45	8.8	0.157	40	7.7	PG+ELG	SE
G12	32248	183.92221	-1.20294	0.085	47	14.9	0.328	45	7.5	ELG+ELG	SE
G12	39055	174.87917	-0.66397	0.096	44	5.2	0.439	40	5.0	ELG+PG	E
G12	39870	178.62517	-0.72424	0.312	40	10.1	0.227	40	6.5	PG+PG	SE
G12	40642	182.30704	-0.78791	0.278	47	12.2	0.184	45	8.6	ELG+ELG	M
G12	53931	175.69525	-0.31443	0.121	47	13.1	0.147	45	12.2	ELG+ELG	SS/F
G12	54130	176.85742	-0.30877	0.326	45	11.6	0.317	47	8.6	ELG+ELG	SE/F
G12	54523	178.36975	-0.30537	0.260	47	10.9	0.077	46	10.0	ELG+ELG	M
G12	55091	180.44258	-0.34558	0.239	40	7.6	0.169	45	7.5	ELG+PG	ES
G12	55175	180.74654	-0.38792	0.357	47	7.0	0.409	47	6.7	ELG+ELG	SE
G12	71072	182.90017	0.17959	0.255	45	6.2	0.122	40	5.6	PG+ELG	SS
G12	71566	185.16637	0.20776	0.287	40	11.5	0.259	47	6.5	ELG+PG	Phi
G12	84090	175.97379	0.48608	0.258	44	8.2	0.284	42	7.2	ELG+PG	SS/M/F
G12	97836	174.84862	0.90228	0.241	40	10.9	0.110	47	8.7	ELG+PG	E
G12	98399	177.78321	0.91949	0.400	40	8.9	0.569	47	7.3	PG+ELG	SE
G12	98624	179.06704	0.99197	0.259	40	11.7	0.270	47	5.5	PG+ELG	E
G12	99508	183.13442	1.00244	0.214	40	9.5	0.744	43	5.0	PG+ELG	M
G12	124295	178.90833	-2.56675	0.280	47	11.2	0.179	44	10.2	ELG+ELG	M
G12	125217	183.07617	-2.50805	0.224	46	7.4	0.265	40	6.0	ELG+PG	E
G12	130303	176.78942	-2.18512	0.435	47	7.7	0.398	40	7.5	PG+ELG	SE
G12	130523	177.73192	-2.10683	0.163	47	10.9	0.249	44	9.6	ELG+ELG	SE
G12	131725	182.36783	-2.24046	0.630	46	9.7	0.179	40	8.2	PG+ELG	E
G12	136782	176.11142	-1.77261	0.394	40	7.0	0.246	46	6.8	ELG+PG	SE
G12	136800	176.05287	-1.77459	0.264	40	11.7	0.589	47	7.8	PG+ELG	M
G12	136907	176.30279	-1.74244	0.028	47	11.3	0.256	45	7.6	ELG+ELG	SE
G12	137783	179.51112	-1.69882	0.097	47	10.9	0.268	45	8.8	ELG+ELG	M/SS
G12	138015	180.50629	-1.65407	0.267	40	10.9	0.250	47	5.2	ELG+PG	E
G12	138368	181.94588	-1.82568	0.304	45	8.3	0.274	47	6.3	ELG+ELG	E
G12	138811	184.17454	-1.81681	0.450	47	8.6	0.074	45	5.9	ELG+ELG	S
G12	164640	178.14021	-2.71487	0.078	40	11.6	0.153	45	6.7	PG+ELG	SS
G12	164995	179.40017	-2.87571	0.267	45	9.5	0.270	46	8.0	ELG+ELG	Q
G12	172153	181.44675	-2.44182	0.514	43	6.2	0.567	42	5.5	ELG+PG	SE
G12	177278	176.08696	-1.86907	0.316	43	5.8	0.385	45	5.1	ELG+ELG	M
G12	184530	176.70954	-1.43849	0.391	40	10.3	0.156	45	9.7	ELG+PG	SE
G12	185604	180.96967	-1.46278	0.265	40	10.6	0.273	47	9.5	PG+ELG	SE/F
G12	185812	181.78058	-1.54840	0.313	47	10.1	0.181	46	9.4	ELG+ELG	ES
G12	185998	182.60063	-1.61024	0.414	40	9.0	0.288	45	7.4	ELG+PG	ES
G12	186085	182.89554	-1.64913	0.241	45	7.6	0.380	40	7.0	ELG+PG	E
G12	186516	184.85638	-1.53982	0.324	40	9.2	0.265	45	5.8	ELG+PG	SE/F
G12	186737	185.59350	-1.49532	0.301	43	8.1	0.297	45	5.9	ELG+ELG	M

Table 4. – *continued.*

Field	GAMA-id	RA	DEC	$z$	T1	$r_x$	$z_2$	T2	$r_{x,2}$	Spec. Type	Vis. Type
G12	220204	180.67683	1.56371	0.353	42	8.0	0.228	47	6.5	ELG+PG	ES
G12	220682	182.74350	1.59787	0.289	40	9.8	0.361	47	9.8	PG+ELG	Ef
G12	220854	183.53083	1.55306	0.266	40	9.6	0.327	46	9.2	PG+ELG	SE
G12	230803	181.08337	1.93953	0.166	44	10.2	0.243	45	9.2	ELG+ELG	ES
G12	231043	182.16688	1.99840	0.160	40	10.1	0.689	47	8.9	PG+ELG	Ef
G12	231307	183.15171	1.97018	0.190	40	12.2	0.218	47	6.7	PG+ELG	Ef
G12	231746	185.33296	1.92256	0.423	40	9.5	0.460	47	6.9	PG+ELG	ES/Ef
G12	231768	185.44796	1.94621	0.226	44	11.3	0.252	47	8.7	ELG+ELG	ES
G12	231785	185.53046	1.88483	0.112	44	9.1	0.346	47	6.4	ELG+ELG	M
G12	272227	178.47396	1.32070	0.078	47	10.2	0.230	44	10.1	ELG+ELG	SE
G12	272828	180.97808	1.42330	0.402	40	9.9	0.238	47	6.9	ELG+PG	Phi
G12	273903	185.65375	1.33724	0.217	40	10.1	0.415	46	6.6	PG+ELG	E
G12	289050	180.98801	1.78262	0.262	43	12.5	0.259	45	6.6	ELG+ELG	M
G12	289265	181.63046	1.82378	0.295	40	9.1	0.292	40	7.3	PG+PG	ES
G12	289278	181.64301	1.74123	0.294	42	10.9	0.701	45	5.0	PG+ELG	ES
G12	396570	174.04408	1.44452	0.454	47	8.1	0.077	44	6.7	ELG+ELG	S/M
G12	397097	176.71996	1.48606	0.156	40	8.5	0.152	44	6.5	ELG+PG	SE/F
G12	402278	174.23017	1.89732	0.138	40	10.2	0.204	45	5.7	PG+ELG	SS
G12	537363	184.95279	-0.87211	0.040	46	7.5	0.206	40	7.2	ELG+PG	SE/B
G12	559147	175.88608	-0.43995	0.351	40	9.9	0.803	42	5.4	PG+PG	EE
G12	559653	177.75950	-0.47629	0.124	44	10.1	0.259	44	9.4	ELG+ELG	SS/F
G12	560010	178.85871	-0.57989	0.225	47	12.0	0.054	47	9.7	ELG+ELG	SS/M
G12	560475	180.41129	-0.48254	0.165	40	9.9	0.543	47	6.5	PG+ELG	EE
G12	560853	181.98808	-0.52788	0.224	40	7.1	0.682	47	5.4	PG+ELG	Ef
G12	583469	175.01863	-0.14991	0.314	40	11.2	0.747	47	7.4	PG+ELG	Ef
G12	583813	176.83237	-0.16391	0.137	45	7.3	0.109	47	5.9	ELG+ELG	Ef
G12	585446	182.74083	-0.13542	0.345	42	7.5	0.331	40	6.3	PG+PG	SE
G12	585644	183.83021	-0.19625	0.404	40	9.4	0.256	46	7.8	ELG+PG	EE/Ef
G12	586392	184.62887	-0.18264	0.456	45	7.8	0.307	40	6.5	PG+ELG	Ef
G12	586648	185.72429	-0.20906	0.697	47	10.3	0.287	40	9.7	PG+ELG	Ef
G12	610029	178.25696	0.30019	0.365	40	9.0	0.391	47	5.7	PG+ELG	SE
G12	610529	180.54204	0.39134	0.256	45	11.3	0.701	47	7.3	ELG+ELG	Ef
G12	690020	179.39604	-1.13984	0.263	40	8.8	0.348	47	6.4	PG+ELG	ES/Q
G12	746445	179.08296	-0.20491	0.107	40	9.7	0.645	42	5.5	PG+PG	EE
G12	787196	177.01971	-1.87064	0.323	47	9.3	0.116	44	7.5	ELG+ELG	M
G12	814991	181.52958	1.93496	0.223	40	8.3	0.297	44	5.3	PG+ELG	Ef
G12	947988	177.90113	-1.11874	0.295	44	7.4	0.136	45	6.3	ELG+ELG	SS
G15	14983	213.63450	0.74998	0.273	40	10.4	0.528	47	9.5	PG+ELG	EE
G15	15221	214.61879	0.62943	0.232	40	10.9	0.279	47	7.7	PG+ELG	SE
G15	15554	215.97479	0.67592	0.142	40	7.7	0.227	46	6.4	PG+ELG	SE
G15	17244	222.50238	0.81555	0.447	40	7.2	0.496	42	4.7	PG+PG	SE
G15	48883	218.90542	-0.74389	0.343	46	9.1	0.245	40	8.6	PG+ELG	SE
G15	62459	213.06783	-0.25768	0.187	44	7.7	0.424	40	6.5	ELG+PG	E
G15	63082	214.46454	-0.30878	0.251	47	12.3	0.124	45	8.8	ELG+ELG	SS/B
G15	64181	218.48892	-0.31288	0.403	40	7.5	0.214	46	7.4	ELG+PG	ES
G15	65016	221.17254	-0.29001	0.239	46	12.9	0.286	46	11.0	ELG+ELG	S
G15	65298	222.49875	-0.40713	0.253	40	8.7	0.649	47	8.3	PG+ELG	E
G15	77892	215.20808	0.17706	0.316	40	9.0	0.620	45	5.7	PG+ELG	E
G15	78841	218.90942	0.12274	0.218	40	12.1	0.215	47	5.1	ELG+PG	ES
G15	92523	216.62879	0.62516	0.125	46	7.9	0.100	47	7.5	ELG+ELG	S
G15	106821	217.32700	0.86711	0.160	40	9.8	0.452	47	6.2	PG+ELG	E
G15	238715	215.06083	1.60423	0.190	40	11.0	0.243	45	9.3	PG+ELG	M
G15	239143	216.51021	1.60820	0.084	45	8.6	0.294	44	5.9	ELG+ELG	S
G15	239367	217.45604	1.52598	0.284	40	10.2	0.379	45	8.5	PG+ELG	ES
G15	239721	218.71629	1.60518	0.199	47	9.6	0.056	47	8.9	ELG+ELG	SE/B
G15	240564	223.16475	1.38699	0.213	45	9.3	0.275	47	6.2	ELG+ELG	SE/Ef
G15	249903	213.33275	2.02850	0.176	47	9.7	0.179	43	7.1	ELG+ELG	S
G15	250209	214.17046	2.07386	0.553	47	7.1	0.386	40	6.6	PG+ELG	Ef
G15	250487	214.82401	2.12522	0.304	44	7.1	0.269	40	5.9	PG+ELG	EE
G15	250796	216.02125	2.13975	0.199	40	10.2	0.132	45	6.4	ELG+PG	Ef
G15	251342	218.22696	1.97782	0.439	40	7.1	0.466	43	5.8	PG+ELG	EE
G15	251526	219.06642	1.97840	0.063	46	8.5	0.283	45	7.5	ELG+ELG	S/M

**Table 4.** – *continued.*

Field	GAMA-id	RA	DEC	$z$	T1	$r_x$	$z_2$	T2	$r_{x,2}$	Spec. Type	Vis. Type
G15	262626	220.31992	2.41527	0.287	40	6.9	0.028	44	6.0	ELG+PG	SE/B
G15	262987	222.23792	2.38034	0.562	42	7.6	0.207	40	7.1	PG+PG	ES/Ef
G15	266240	216.94617	2.79181	0.297	45	6.1	0.378	40	5.3	ELG+PG	ES
G15	278240	215.80875	1.07883	0.393	44	7.9	0.282	47	5.4	ELG+ELG	EE
G15	296898	213.92688	1.53891	0.160	40	11.0	0.045	47	8.5	ELG+PG	M/Ef
G15	297627	216.43496	1.38861	0.453	47	7.8	0.197	47	7.2	ELG+ELG	SS/M
G15	297645	216.57825	1.38436	0.316	47	12.8	0.004	44	6.3	ELG+ELG	SE/M
G15	298302	219.30533	1.41623	0.403	40	6.5	0.150	40	6.0	PG+PG	EE
G15	298316	219.34801	1.28769	0.333	40	7.4	0.329	40	6.8	PG+PG	ES
G15	298899	222.14058	1.16504	0.319	40	7.0	0.374	47	6.3	PG+ELG	E
G15	319348	214.14233	1.86348	0.266	40	8.6	0.286	46	7.2	PG+ELG	SE
G15	319416	214.38538	1.91140	0.051	40	8.3	0.245	43	6.5	PG+ELG	S
G15	320078	216.84646	1.88291	0.348	42	7.5	0.292	42	7.5	PG+PG	EE/M
G15	320384	218.13475	1.68924	0.109	40	8.4	0.192	46	7.8	PG+ELG	SS
G15	320557	218.63421	1.78566	0.274	40	11.1	0.279	46	7.2	PG+ELG	EE
G15	320705	219.18917	1.74384	0.176	44	8.1	0.546	47	6.6	ELG+ELG	S
G15	321208	221.87658	1.67057	0.358	40	7.8	0.286	46	5.2	ELG+PG	EE
G15	342308	215.06900	2.22422	0.391	45	9.6	0.328	40	5.9	PG+ELG	SE
G15	343868	222.41704	2.17379	0.121	47	14.4	0.124	47	7.9	ELG+ELG	SS
G15	362394	214.88958	2.70961	0.394	42	7.9	0.315	40	6.4	PG+PG	E/Ef
G15	367197	220.31267	2.92665	0.212	40	6.8	0.098	44	5.9	ELG+PG	Ef
G15	460386	211.94129	-1.80552	0.113	46	8.5	0.516	43	8.5	ELG+ELG	SE
G15	460463	212.48058	-1.61746	0.115	40	10.8	0.411	47	6.8	PG+ELG	SE/Ef
G15	460713	213.41046	-1.64736	0.429	47	9.4	0.308	40	6.4	PG+ELG	ES
G15	463638	213.94213	-1.18728	0.050	47	10.6	0.149	47	8.1	ELG+ELG	SE
G15	485756	217.11896	-1.79492	0.269	40	11.5	0.404	47	6.2	PG+ELG	EE
G15	493692	221.98950	-1.36708	0.261	47	13.0	0.147	45	8.5	ELG+ELG	SS
G15	508116	215.95117	-1.68131	0.202	40	7.8	0.305	44	6.9	PG+ELG	ES/Ef
G15	508211	216.27379	-1.59829	0.289	40	8.4	0.278	47	6.7	ELG+PG	SE
G15	512280	218.33704	-1.05040	0.179	45	9.2	0.030	47	8.8	ELG+ELG	SS/B
G15	513306	223.07412	-1.01726	0.211	46	11.3	0.320	42	8.2	ELG+PG	ES/Ef
G15	543716	212.59971	-0.92718	0.357	47	8.3	0.204	44	6.6	ELG+ELG	SS
G15	544875	217.28529	-0.94940	0.394	42	8.1	0.494	40	5.3	PG+PG	EE
G15	544985	217.81129	-0.90871	0.402	40	8.4	0.400	45	5.4	ELG+PG	Ef
G15	545139	218.38854	-1.00978	0.241	46	6.5	0.323	40	6.0	ELG+PG	SE
G15	545712	220.81617	-0.88778	0.450	42	9.4	0.216	46	7.2	ELG+PG	ES/M
G15	570323	223.22658	-0.58658	0.313	45	13.3	0.280	47	5.5	ELG+ELG	ES/Ef
G15	592207	212.01942	-0.07878	0.256	40	8.3	0.178	40	7.3	PG+PG	Ef
G15	617535	211.95117	0.23064	0.510	47	8.0	0.262	40	6.0	PG+ELG	Ef
G15	617856	213.49346	0.35214	0.231	40	11.7	0.262	47	6.7	PG+ELG	SE
G15	618687	216.50154	0.23066	0.150	47	13.2	0.084	47	9.5	ELG+ELG	SS
G15	884103	217.42279	-1.68879	0.793	47	8.5	0.018	47	7.4	ELG+ELG	SS
G02	1126606	33.89513	-6.55139	0.217	40	9.8	0.749	43	5.1	PG+ELG	SE
G02	1217811	33.60950	-4.23305	0.181	40	7.1	0.154	44	6.6	ELG+PG	Phi
G02	1270758	32.65929	-10.07633	0.144	40	9.7	0.698	43	5.6	PG+ELG	S
G02	1274050	32.82713	-9.86427	0.161	44	6.9	0.507	47	6.5	ELG+ELG	SS/Phi
G02	1298084	32.37917	-6.37684	0.238	47	6.1	0.273	40	6.0	ELG+PG	EE
G02	1312058	32.29279	-5.43011	0.417	40	8.2	0.619	47	7.1	PG+ELG	Ef
G02	1320592	32.94087	-4.82006	0.070	47	11.7	0.162	46	10.0	ELG+ELG	SE
G02	1440776	31.98304	-4.41341	0.209	45	6.3	0.640	40	5.9	ELG+PG	EE
G02	1537351	30.80412	-6.04563	0.424	40	6.6	0.622	42	6.5	PG+PG	EE
G02	1568229	30.69258	-4.13571	0.291	40	5.9	0.413	40	5.8	PG+PG	ES/Ef
G02	1569977	30.69342	-4.01222	0.331	40	10.3	0.436	47	5.3	PG+ELG	Ef
G02	1614527	35.88917	-8.47218	0.283	40	11.6	0.195	45	5.1	ELG+PG	Ef/S
G02	1675035	35.41175	-4.48197	0.258	40	7.7	0.080	46	5.8	ELG+PG	Ef/ES
G02	1684064	35.62492	-3.87688	0.614	47	8.4	0.292	40	6.6	PG+ELG	SE/M
G02	1726233	36.65454	-8.52167	0.184	47	10.3	0.155	47	5.4	ELG+ELG	S
G02	1740396	36.36688	-9.35231	0.196	47	12.3	0.445	40	6.3	ELG+PG	SE
G02	1760310	35.95496	-6.11922	0.236	45	11.2	0.144	45	8.3	ELG+ELG	SS
G02	1763319	36.37075	-5.91766	0.294	40	7.2	0.319	44	6.6	PG+ELG	SS
G02	1765570	36.16213	-5.76612	0.231	40	7.4	0.162	44	6.3	ELG+PG	ES
G02	1771132	36.28483	-5.39210	0.297	46	10.1	0.231	44	6.9	ELG+ELG	S/M
G02	1779869	36.29463	-4.84248	0.309	44	6.2	0.460	46	5.8	ELG+ELG	EE



Table 4. – *continued.*

Field	GAMA-id	RA	DEC	$z$	T1	$r_x$	$z_2$	T2	$r_{x,2}$	Spec. Type	Vis. Type
G02	1988308	38.11142	-5.96424	0.300	47	8.2	0.303	47	7.4	ELG+ELG	SS
G02	2002618	38.30588	-5.07329	0.348	42	9.7	0.256	45	6.2	ELG+PG	SE
G02	2005629	37.92875	-4.88681	0.189	40	6.9	0.716	45	5.9	PG+ELG	SE/S
G02	2007752	38.48246	-4.76219	0.355	47	8.4	0.034	44	6.0	ELG+ELG	S
G02	2248952	30.82808	-7.63584	0.242	40	5.4	0.328	45	5.2	PG+ELG	ES
G02	2308869	35.92083	-4.02211	0.237	47	11.2	0.264	47	10.1	ELG+ELG	SS
G02	2379807	37.16025	-4.03447	0.333	40	10.8	0.329	46	8.6	ELG+PG	Ef
G23	5000687	344.09237	-34.88054	0.199	42	8.7	0.326	47	7.5	PG+ELG	-
G23	5006684	343.38587	-33.71781	0.219	40	9.6	0.208	47	8.5	ELG+PG	-
G23	5014213	350.01962	-32.35935	0.202	42	10.3	0.785	43	6.0	PG+ELG	-
G23	5022159	347.44408	-31.04443	0.213	40	8.0	0.235	45	6.1	PG+ELG	-
G23	5026858	340.90525	-30.26776	0.151	40	8.4	0.282	44	5.5	PG+ELG	-
G23	5027548	341.34442	-30.14947	0.282	46	8.5	0.311	47	6.8	ELG+ELG	-
G23	7014061	343.38537	-33.71829	0.208	46	9.9	0.224	40	8.0	ELG+PG	-
G23	7019633	349.60625	-33.45856	0.165	40	8.7	0.187	40	8.3	PG+PG	-
G23	7021723	345.68529	-33.36733	0.221	40	10.8	0.319	47	6.9	PG+ELG	-
G23	7023086	346.05408	-33.30514	0.212	40	7.8	0.188	45	7.0	ELG+PG	-
G23	7028850	342.77721	-33.04329	0.321	40	6.6	0.328	47	6.2	PG+ELG	-
G23	7032116	341.93799	-32.92324	0.672	40	7.0	0.476	40	6.5	PG+PG	-
G23	7035191	346.47717	-32.81103	0.634	43	8.0	0.188	40	5.9	PG+ELG	-
G23	7046392	343.18829	-32.36551	0.289	40	9.3	0.116	46	6.0	ELG+PG	-
G23	7048497	342.86779	-32.27196	0.239	45	6.2	0.389	45	5.7	ELG+ELG	-
G23	7056621	342.57587	-31.90962	0.388	40	6.6	0.425	47	6.2	PG+ELG	-
G23	7061088	342.12237	-31.71619	0.240	40	7.7	0.243	44	6.6	PG+ELG	-
G23	7069205	342.01071	-31.37594	0.261	46	8.9	0.432	40	6.5	ELG+PG	-
G23	7070361	350.69167	-31.32483	0.264	47	7.3	0.268	47	5.5	ELG+ELG	-
G23	7073988	346.66158	-31.16843	0.162	47	12.4	0.068	47	8.9	ELG+ELG	-
G23	7073990	346.66237	-31.16836	0.068	47	12.2	0.162	46	7.8	ELG+ELG	-
G23	7076874	346.36892	-31.04973	0.270	40	8.4	0.088	45	7.5	ELG+PG	-
G23	7081863	340.21004	-30.82531	0.287	45	9.6	0.217	40	8.5	PG+ELG	-
G23	7083868	343.97800	-30.75893	0.359	40	6.7	0.722	47	6.6	PG+ELG	-
G23	7093351	344.23937	-30.36704	0.449	40	7.7	0.325	47	7.2	ELG+PG	-